

## ACCURATE DETERMINATION OF THE MASS DISTRIBUTION IN SPIRAL GALAXIES. II. TESTING THE SHAPE OF DARK HALOS

SÉBASTIEN BLAIS-OUELLETTE<sup>1</sup>

Département de physique and Observatoire du mont Mégantic, Université de Montréal, CP 6128, Station Centreville, Montreal, Quebec, H3C 3J7, Canada;  
and Laboratoire d'Astrophysique de Marseille, 2 Place Le Verrier, F-13248 Marseille Cedex 4, France; blaisous@llnl.gov

PHILIPPE AMRAM

Laboratoire d'Astrophysique de Marseille, 2 Place Le Verrier, F-13248 Marseille Cedex 4, France; amram@observatoire.cnrs-mrs.fr

AND

CLAUDE CARIGNAN<sup>2</sup>

Département de physique and Observatoire du mont Mégantic, Université de Montréal, CP 6128, Station Centreville, Montreal, Quebec, H3C 3J7, Canada;  
carignan@astro.umontreal.ca

Received 2000 July 10; accepted 2000 December 27

### ABSTRACT

New high-resolution Fabry-Perot data at the Canada-France-Hawaii Telescope combined with published VLA 21 cm observations are used to determine the mass distribution of NGC 3109 and IC 2574. The multiwavelength rotation curves allow us to test with confidence different dark halo functional forms from the pseudoisothermal sphere to some popular halo distributions motivated by cold dark matter  $N$ -body simulations. It appears that the density distributions with high central concentration, predicted by these simulations, are very hard to reconcile with rotation curves of late-type spiral galaxies. Modified Newtonian dynamics (MOND) is also considered a potential solution to missing mass and is tested the same way. Using the higher resolution H $\alpha$  data and new H I data for NGC 3109, one can see that MOND can reproduce in detail the rotation curves of IC 2574 and NGC 3109. However, the value for the MOND universal constant is  $\sim 2$  times larger than the value found for more massive spiral galaxies.

*Key words:* dark matter — galaxies: fundamental parameters —  
galaxies: individual (IC 2574, NGC 3109, NGC 3198, NGC 5585) —  
techniques: interferometric

*On-line material:* color figures

### 1. INTRODUCTION

Over the last 30 years, rotation curves have been a very efficient tool to study the mass distribution in spiral galaxies. They clearly brought to light the important discrepancy between the luminous mass and the gravitational mass that has led to the supposition of a large amount of dark matter in the universe. The now commonly accepted picture is that this unseen matter takes the form of large halos in the center of which galaxies are embedded. Alternatively, the gravitational attraction could deviate from the pure Newtonian force at very low acceleration so that no dark matter is necessary.

The resolution reached by  $N$ -body simulations of the cosmic evolution of dark halos (Navarro, Frenk, & White 1996b, 1997; Fukushige & Makino 1997; Moore et al. 1998; Kravtsov et al. 1998) allows one to predict the inner part of halo-density profiles. In theory, these profiles could be directly compared with the ones deduced from modeling the rotation curves. Unfortunately, the sensitivity of the rotation curves to the exact density profile of the halos is quite low, and one must use the highest sensitivity and the highest resolution possible to arrive at useful comparisons (Blais-Ouellette et al. 1999, hereafter Paper I).

This study primarily investigates in the context of Newtonian gravitation the density profiles of the dark halos of two late-type spiral galaxies: NGC 3109 and IC 2574. As late type, their bulge is minimal, making them well-suited objects for sensitive mass distribution studies because of the reduced uncertainties due to the negligible spheroid contribution in the inner parts. Mass models of NGC 3109 based on radio observations have already been presented by Jobin & Carignan (1990), while the dark matter distribution in IC 2574 has been studied by Martimbeau, Carignan, & Roy (1994). New high-resolution Fabry-Perot observations of the H $\alpha$  emission line are used in combination with published 21 cm data to form accurate multiwavelength rotation curves. These curves are used to model the mass distribution in the galaxies. The models include a stellar disk, a gaseous component, and a dark spherical halo.

Moreover, NGC 3109 has often been presented as a test for modified Newtonian dynamics (MOND; Milgrom 1983). As noted in Broeils (1992), the inner part of the rotation curve is crucial to draw any conclusion on the MOND fit to this galaxy. Therefore, the mass models of the two galaxies based on the MOND assumption are presented as well.

The CFHT Fabry-Perot observations are described in § 2, while the mass models of the two galaxies, to which we add NGC 5585 and NGC 3198 from Paper I, are discussed in § 3.

### 2. NEW FABRY-PEROT OBSERVATIONS

The Fabry-Perot observations of the H $\alpha$  emission line

<sup>1</sup> Current address: Institute of Geophysics and Planetary Physics, Lawrence Livermore National Laboratory, P.O. Box 808, L-413, Livermore, CA 94551-9900.

<sup>2</sup> Visiting astronomer, Canada-France-Hawaii Telescope, operated by the National Research Council of Canada, the Centre National de la Recherche Scientifique de France, and the University of Hawaii.

were obtained in 1994 February at the Canada-France-Hawaii Telescope (CFHT). The etalon (CFHT1) was installed in the CFHT's multiobject spectrograph (MOS). A narrowband filter ( $\Delta\lambda \approx 12 \text{ \AA}$ ), centered at  $\lambda_0 = 6565.5 \text{ \AA}$  for NGC 3109 ( $V_{\text{sys}} \approx 402 \text{ km s}^{-1}$ ) and at  $\lambda_0 = 6559.5 \text{ \AA}$  for IC 2574 ( $V_{\text{sys}} \approx 53 \text{ km s}^{-1}$ ), was placed in front of the etalon. The available field with no vignetting was  $\approx 8.5 \times 8.5$ , with  $0''.314 \text{ pixel}^{-1}$ . The pixels were binned  $3 \times 3$  to increase the signal-to-noise ratio and minimize the readout time. The free spectral range of  $5.66 \text{ \AA}$  ( $259 \text{ km s}^{-1}$ ) was scanned in 27 (plus 1 overlapping) channels, giving a sampling of  $0.21 \text{ \AA}$  ( $9.6 \text{ km s}^{-1}$ ) per channel. Eight minutes integration were spent at each channel position. Table 1 lists the complete observing parameters.

Following normal debiasing and flat-fielding with standard IRAF procedures, a robust three-dimensional cosmic-ray removal routine that tracks cosmic rays by spatial (pixel to pixel) and spectral (frame to frame) analysis was applied. Ghost reflections were then removed using the technique described in Paper I. With the ADHOC software package,<sup>3</sup> photometric variations were corrected using the mean night sky (background + emission lines) to calculate the corrections to apply to each frame. Then a calibration based on a neon lamp ( $\lambda = 6598.95 \text{ \AA}$ ) was used to fix the zero point of the spectrum at each pixel.

### 2.1. NGC 3109

Table 2 gives the optical parameters of NGC 3109. In order to get a sufficient signal-to-noise ratio throughout the velocity fields, two different Gaussian spatial smoothings ( $\sigma = 3.5$  and  $5$  pixels) were performed on the cube (all the channels). Velocity maps were then obtained from the intensity-weighted means of the H $\alpha$  peaks to determine the radial velocity for each pixel. A final variable-resolution

TABLE 2  
PARAMETERS OF NGC 3109

Parameter	Value
Morphological type <sup>a</sup> .....	SBm
R.A. (J2000.0) .....	10 <sup>h</sup> 03 <sup>m</sup> 06 <sup>s</sup> .6
Decl. (J2000.0) .....	-26°09'32"
$l$ .....	262°1
$b$ .....	23°1
Adopted distance (Mpc) <sup>b</sup> .....	1.36 ( $1' \approx 0.4 \text{ kpc}$ )
Mean axis ratio, $q = b/a^c$ .....	$0.28 \pm 0.02$
Inclination, $i^c$ .....	$75^\circ \pm 2^\circ$
Isophotal major diameter, $D_{25}^c$ .....	14.4
Major axis P.A. <sup>c</sup> .....	$93^\circ \pm 2^\circ$
Exponential scale length (kpc) <sup>c</sup> .....	1.2
Holmberg radius, $R_{\text{Ho}}^c$ .....	13.3
Absolute magnitude, $M_B^c$ .....	-16.35
Total luminosity, $L_B$ .....	$5.2 \times 10^8 L_\odot$
Heliocentric radial velocity ( $\text{km s}^{-1}$ ) <sup>c</sup> .....	$404 \pm 3$

<sup>a</sup> de Vaucouleurs et al. 1991.

<sup>b</sup> Musella et al. 1997.

<sup>c</sup> Jobin & Carignan 1990.

velocity map (Fig. 1, top) was built, keeping higher resolution for regions with originally higher signal-to-noise ratios. The full-resolution H $\alpha$  image is also shown in the lower part of Figure 1.

The rotation curve was obtained from the velocity field by using two different methods. First, an estimate was made using the task ROCUR (Begeman 1987; Côté, Carignan, & Sancisi 1991) in the AIPS package, where annuli, tilted with respect to the plane of the galaxy (ellipses in the plane of the sky), are fitted to the velocity field, minimizing the dispersion inside each annulus. The dynamical center, systemic velocity, position angle, and inclination were estimated this way. Second, the ADHOC package was used to fine-tune these parameters by comparison of both sides of the galaxy and examination of the residual velocity field (see Amram et al. 1992 for the detailed method). The systemic velocity was found to be  $402 \text{ km s}^{-1}$ , very close to the value of  $404 \text{ km s}^{-1}$  found with the H I observations of Jobin & Carignan (1990). Since a warp is clearly present even in the optical velocity field, the final rotation curve was derived with ROCUR, leaving the inclination and the position angle free to vary. In this context, the slightly high value of the first velocity point can be understood as a product of the poor determination of the inclination in the center of the galaxy. Table 3 gives the full rotation curve at  $20''$  resolution, while Figure 2 illustrates the rotation curve, as well as the variation of inclination and position angle. Following Jobin & Carignan (1990), the rotation curve was corrected for asymmetric drift.

Currently, no convention on the way to represent the errors on rotation curves exists in the literature. Error bars are often simply given as the velocity dispersion in the ring used at each radius. However, warm gas is known to be more sensitive to its environment than cold gas. Turbulence, local density variations (such as spiral arms and bars), and winds from stars and supernovae of the young stellar-forming regions in which the ionized gas is found increase its dispersion. This can lead to the paradox that the fewer points you have (as in long-slit observations), the lower is your dispersion and the smaller are your error bars. As a more direct probe of the uncertainties on the measured potential, the difference between the two sides of the galaxy

<sup>3</sup> See <http://www-obs.cnrs-mrs.fr/adhoc/adhoc.html>.

TABLE 1  
PARAMETERS OF THE FABRY-PEROT OBSERVATIONS

Parameter	Value
Dates .....	1994 February 21 and 22
Telescope .....	3.6 m CFHT
Instrumentation:	
Focal plane instrument .....	MOSFP
CCD detector .....	$2048 \times 2048 \text{ Loral3}$ , $\sigma = 8e^{-1}$
Fabry-Perot etalon .....	Scanning QW1162 (CFHT1)
Interference order .....	1155 at neon $\lambda$
Mean finesse in the field .....	12
Calibration lamp .....	Neon ( $\lambda = 6598.95 \text{ \AA}$ )
Duration NGC 3109:	
Per channel .....	7.28 minutes
Total .....	3 hr 24 minutes
Filter .....	$\lambda_0 = 6565.5 \text{ \AA}$ , $\Delta\lambda = 12 \text{ \AA}$
Duration IC 2574:	
Per channel .....	8.05 minutes
Total .....	3 hr 45 minutes
Filter .....	$\lambda_0 = 6559.5 \text{ \AA}$ , $\Delta\lambda = 12 \text{ \AA}$
Spatial parameters:	
Field size .....	$8.5 \times 8.5$
Pixel scale .....	$0''.314 \text{ pixel}^{-1}$
Spectral parameters:	
Number of channels .....	27
Free spectral range .....	$5.66 \text{ \AA}$ ( $259 \text{ km s}^{-1}$ )
Sampling .....	$0.21 \text{ \AA}$ ( $9.6 \text{ km s}^{-1}$ ) channel <sup>-1</sup>

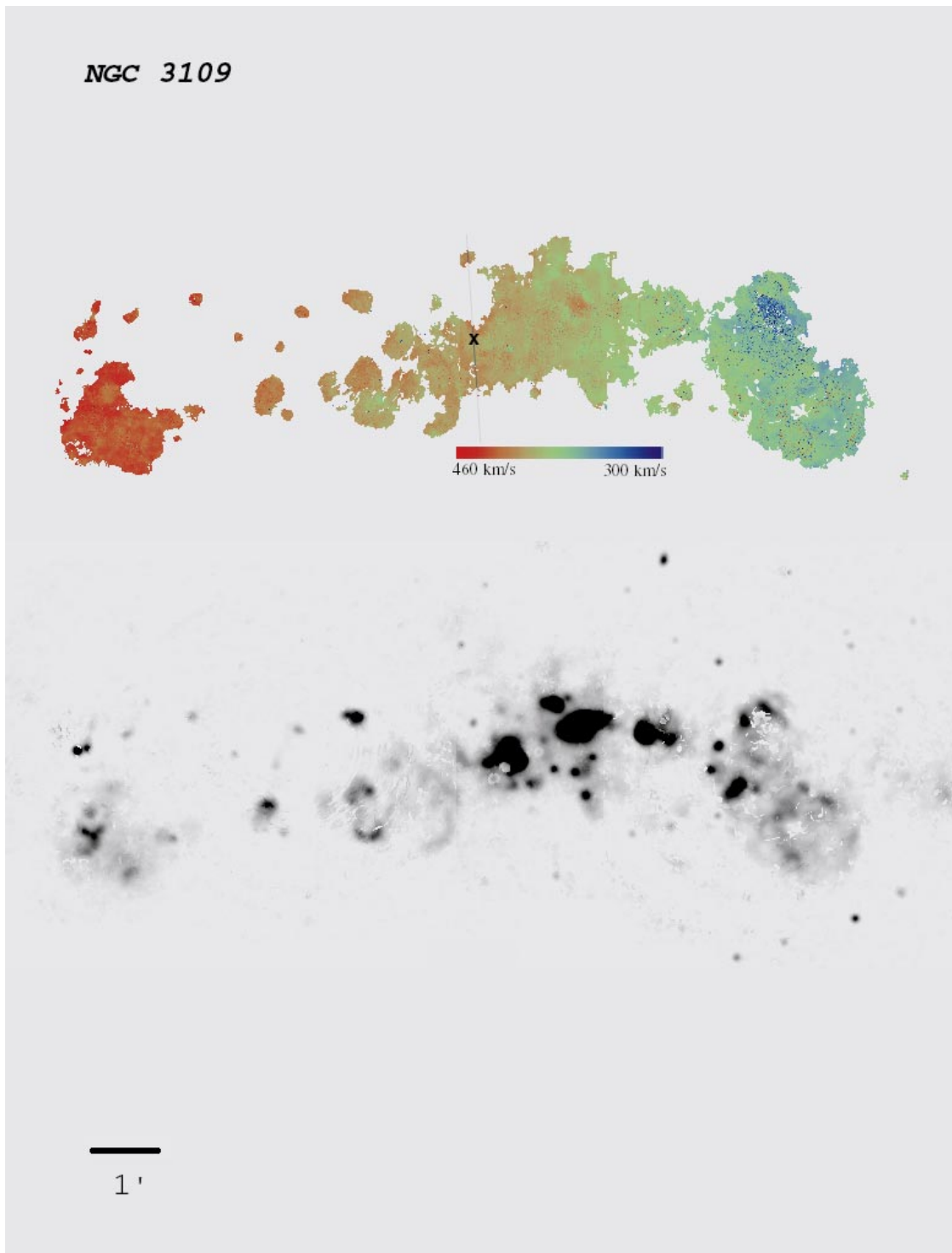


FIG. 1.—Velocity field and H $\alpha$  image of NGC 3109. North is up and east is left. The X and the gray line indicate, respectively, the kinematic center and the axis of separation between the approaching and receding sides.

is often used instead. Some authors will add the error due to uncertainties in inclination and/or position angles.

To differentiate clearly the source of errors, the error bars shown here indicate the error in the mean for each ring ( $\sigma/N^{1/2}$ ), while the solutions for each side of the galaxy are represented by lines (solid for the receding side and dashed for the approaching). Their difference is a good estimate of the asymmetry and large-scale noncircular motions.

The velocity field of NGC 3109 shows many bubble-like features probably due to intense star formation especially

close to the center of the galaxy. The effect of H $\alpha$  bubbles is normally of two kinds: First, if the front and back of a bubble are equally intense and the medium transparent, a broadened or, depending on the resolution, even a doubled H $\alpha$  line can be seen. The true gravitational rotation can still be deduced by averaging the two peaks. However, in many cases only the front of an expanding bubble can be seen, making it difficult to retrieve the true rotational velocities.

In the case of NGC 3109, analysis of the velocity field shows a small deviation from circular motion in the inner

TABLE 3  
OPTICAL ROTATION CURVE OF NGC 3109 AT 20" BINNING  
FROM ROCUR

$R_{\text{sides}}$ (arcsec)	$V_{\text{app}}$ (km s <sup>-1</sup> )	$V_{\text{rec}}$ (km s <sup>-1</sup> )	$R$ (arcsec)	$V$ (km s <sup>-1</sup> )
35.....	8 ± 1	3 ± 1	30	10 ± 2
65.....	6 ± 1	...	70	10 ± 1
95.....	15 ± 1	...	90	15 ± 1
95.....	...	...	110	15 ± 1
125.....	14 ± 1	...	130	15 ± 1
155.....	22 ± 2	...	150	20 ± 1
155.....	...	...	170	25 ± 1
185.....	25 ± 1	...	190	25 ± 1
215.....	26 ± 1	...	210	26 ± 1
215.....	...	...	230	32 ± 1
245.....	32 ± 1	...	250	33 ± 1
275.....	34 ± 1	33 ± 1	270	37 ± 2
275.....	...	...	290	35 ± 2
305.....	35 ± 1	32 ± 135	310	37 ± 2
335.....	39 ± 2	37 ± 1	330	39 ± 2
335.....	...	...	350	41 ± 4
365.....	46 ± 6	40 ± 8	370	49 ± 10
395.....	52 ± 9	42 ± 4	390	47 ± 2
395.....	...	...	410	48 ± 1
425.....	46 ± 2	45 ± 11	...	...

NOTES.—Derived with  $V_{\text{sys}} = 402 \text{ km s}^{-1}$  (see text). The two sides and the global rotational velocities are computed independently. The later are corrected for asymmetric drift.

part of the galaxy. The velocity of the single innermost point of the rotation curve is slightly affected. Despite some peculiar internal velocities, apparently well averaged out, a relatively good agreement can be seen between the two sets of data. The H I velocities (where no beam smearing correction has been applied) were just slightly underestimated in the inner part. This is not really surprising, considering that beam-smearing effects should diminish as the slope of the inner rotation curve diminishes for a given beam width. The multiwavelength rotation curve is thus composed of the H $\alpha$  data points up to 410" and of H I velocities for the rest.

## 2.2. IC 2574

A similar reduction procedure was applied to IC 2574

TABLE 4  
OPTICAL PARAMETERS OF IC 2574

Parameters	Value
Morphological type <sup>a</sup> .....	SABm
R.A. (J2000.0).....	10 <sup>h</sup> 28 <sup>m</sup> 21 <sup>s</sup> .2
Decl. (J2000.0).....	68°24'43"
$l$ .....	140°2
$b$ .....	43°6
Adopted distance (Mpc) <sup>b</sup> .....	3.0 ( $1' \approx 0.8 \text{ kpc}$ )
Mean axis ratio, $q = b/a^b$ .....	0.48 ± 0.06
Inclination, $i^b$ .....	75° ± 3°
Isophotal major diameter, $D_{25}^b$ .....	9.8'
Major axis P.A. <sup>b</sup> .....	52° ± 6°
Exponential scale length (kpc) <sup>b</sup> .....	2.2
Holmberg radius, $R_{\text{HO}}^b$ .....	8'6
Absolute magnitude, $M_B^b$ .....	-16.77
Total luminosity, $L_B$ .....	$8.0 \times 10^8 L_{\odot}$
Heliocentric radial velocity (km s <sup>-1</sup> ) <sup>b</sup> .....	58 ± 3

<sup>a</sup> de Vaucouleurs et al. 1991.

<sup>b</sup> Martimbeau et al. 1994.

(Table 4), and the velocity field is shown juxtaposed with the monochromatic image in Figure 3. It is clear that IC 2574 is more disrupted than NGC 3109. With such a patchy velocity field, a determination of a reliable rotation curve with an iterative method based on velocity dispersion in annuli turned out to be impossible. Direct calculation of the rotation velocity for each pixel was thus done using fixed values for the position angle and the inclination. The dynamical parameters were found by comparing the two sides of the galaxy and by analyzing the residual field. The resulting rotation curve is presented in Table 5, based on a systemic velocity of 53 km s<sup>-1</sup>, a position angle of 52°, and an inclination of 75°, almost identical to the parameters found by Martimbeau et al. (1994) from the H I observations.

The H $\alpha$  rotation curve (Fig. 4) follows more or less the same kind of perturbations as those seen in the H I curve. For example, when one compares the two sides of the H I curve in Figure 8 of Martimbeau et al. (1994), (1) the effect of a giant bubble can clearly be seen at both wavelengths around 240" on the approaching side, (2) the giant north-eastern OB association clearly shows up between 7' and 10' of the receding side, and (3), on the other hand, some probable noncircular motions are seen around 100" in H $\alpha$  but do not show up in H I.

Since the comparison of H I and H $\alpha$  data shows no sign of beam smearing, there would be no reason here to use the disrupted H $\alpha$  curve instead of the 21 cm data as the probe of the gravitational potential of the galaxy.

## 3. MASS MODELS AND PARAMETERS OF THE MASS DISTRIBUTION

### 3.1. Comparison of Different Models Using Standard Gravity

The method used in this paper to model the mass distribution is a slight generalization of the one described in Carignan & Freeman (1985). The luminosity profile, if possible in the near infrared to probe the mass-dominant stellar component, is transformed into a mass distribution for the stellar disk, assuming a variable but radially constant mass-to-light ratio  $[(M/L_B)_*]$  (Casertano 1983; Carignan & Freeman 1985). For the contribution of the gaseous component, the H I radial profile is used, scaled by 1.33 to account for He. The difference between the observed rotation curve and the contribution to the curve from the luminous (stars and gas) component is thus the contribution of the dark component, which can be represented by a dark spherical halo. There are therefore three free parameters, the  $(M/L_B)_*$  for the disk and two parameters for the dark halo: the central density  $\rho_0$  and the core radius,  $r_c$ . A best-fit routine minimizes the  $\chi^2$  in the three-dimensional parameter space.

Many studies approximate later type spiral galaxies such as NGC 3109 and IC 2574 as being totally made of dark matter, neglecting the stellar and gaseous components. This is a good approximation down to a certain radius. However, the innermost parts of the rotation curves are crucial to test the shape of the density profiles. Best-fit models that include the contributions of gas and stars are therefore used to avoid an overestimation of the dark halo contribution.

Following Kravtsov et al. (1998), hereafter KKBP, and Zhao (1996), we use an even broader family of density pro-

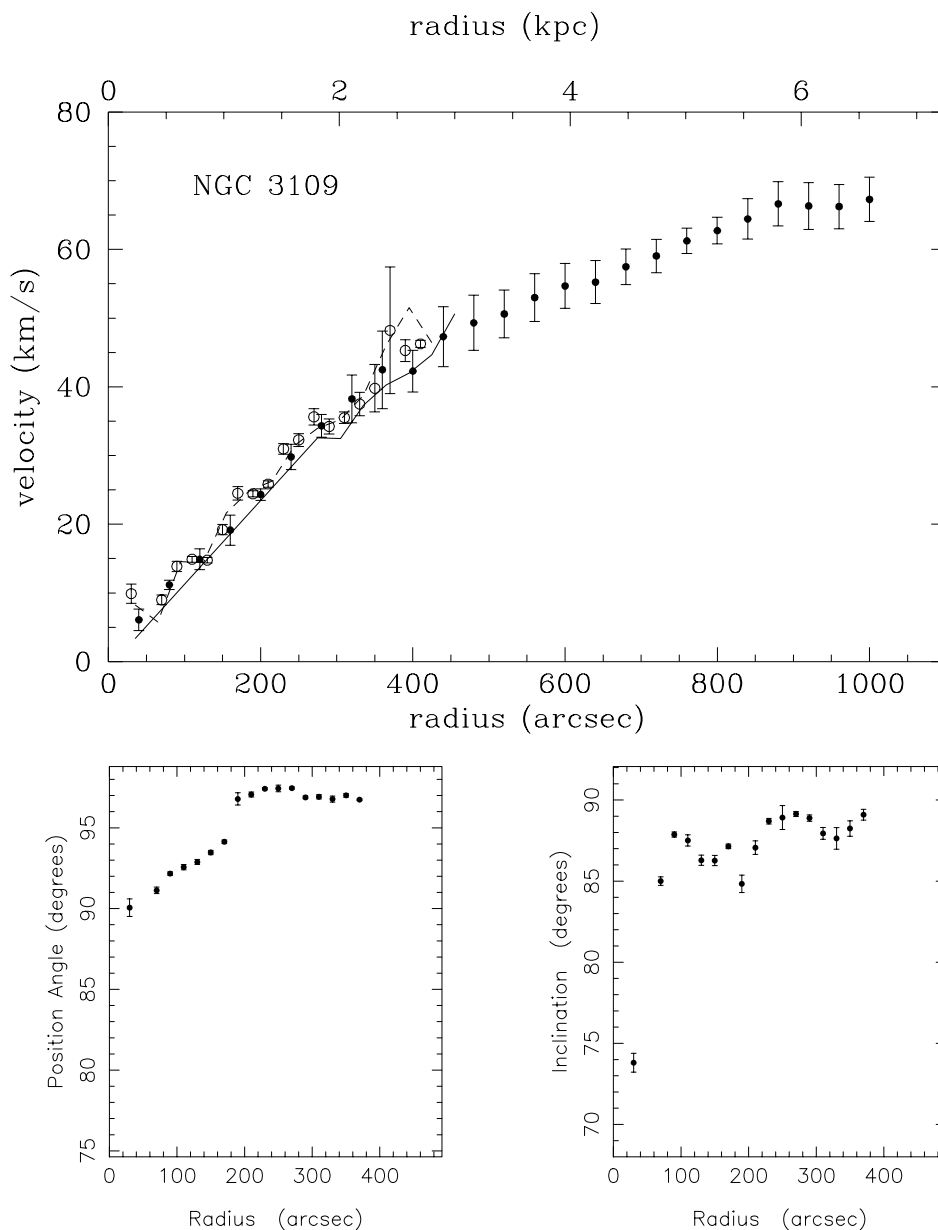


FIG. 2.—*Top*, H $\alpha$  rotation curve of NGC 3109 (*open circles*) compared with the H I rotation curve (*filled circles*) from Jobin & Carignan (1990), showing the approaching (*dashed line*) and receding (*continuous line*) sides; *bottom*, variation with radius of the position angle and inclination for the H $\alpha$  data. See the text for details on curves and error bars.

files for the halo,

$$\rho(r) = \frac{\rho_0}{[c + (r/r_0)^\gamma][1 + (r/r_0)^\alpha]^{(\beta-\gamma)/\alpha}}, \quad (1)$$

where  $\rho_0$  and  $r_0$  are a characteristic density and radius, respectively, and  $c$  can force the presence of a flat-density core. The parameters  $\alpha$ ,  $\beta$ , and  $\gamma$  determine the shape of the density profile.

One can either fit the value of  $(c, \alpha, \beta, \gamma)$  to a particular density profile or set each to a desired value: (1,  $\alpha \neq 0$ , 2, 2) for a pseudoisothermal sphere (Begeman 1987), (0, 1, 3, 1) for an NFW-type halo (Navarro et al. 1996b, hereafter NFW), (1, 2, 3, 1) for halos with the flat-density cores proposed by Burkert (1995), or (0, 2, 3, 0.2) as proposed by KKBP. These four density profiles are presented in Figure

5. Profiles with nonconstant density cores ( $\lim_{r \rightarrow 0} \rho \neq \rho_0$ ), are defined as cuspy. For these profiles, the inner slope is given by  $-\gamma$  and the outer slope by  $\beta$ , while  $\alpha$  controls the sharpness of the turnover point.

NGC 3109 is particularly well suited for dynamical studies. First, its luminous component is minimal ( $B$ -band photometry from Kent 1987) so that the uncertainties related to the unknown mass-to-light ratio of the disk do not have a significant impact. Second, this galaxy is close enough to allow direct distance estimation via multicolor observations of a large number of Cepheids (Musella, Piotto, & Capaccioli 1997). The adopted distance is 1.36 Mpc.

In Figures 6 and 7, best-fit models are given for the rotation curves of NGC 3109 and IC 2574, respectively. The high-resolution data (used up to 410'' for NGC 3109) remove some uncertainties pointed out by Navarro (1997) in the differences between H I curves from different gener-

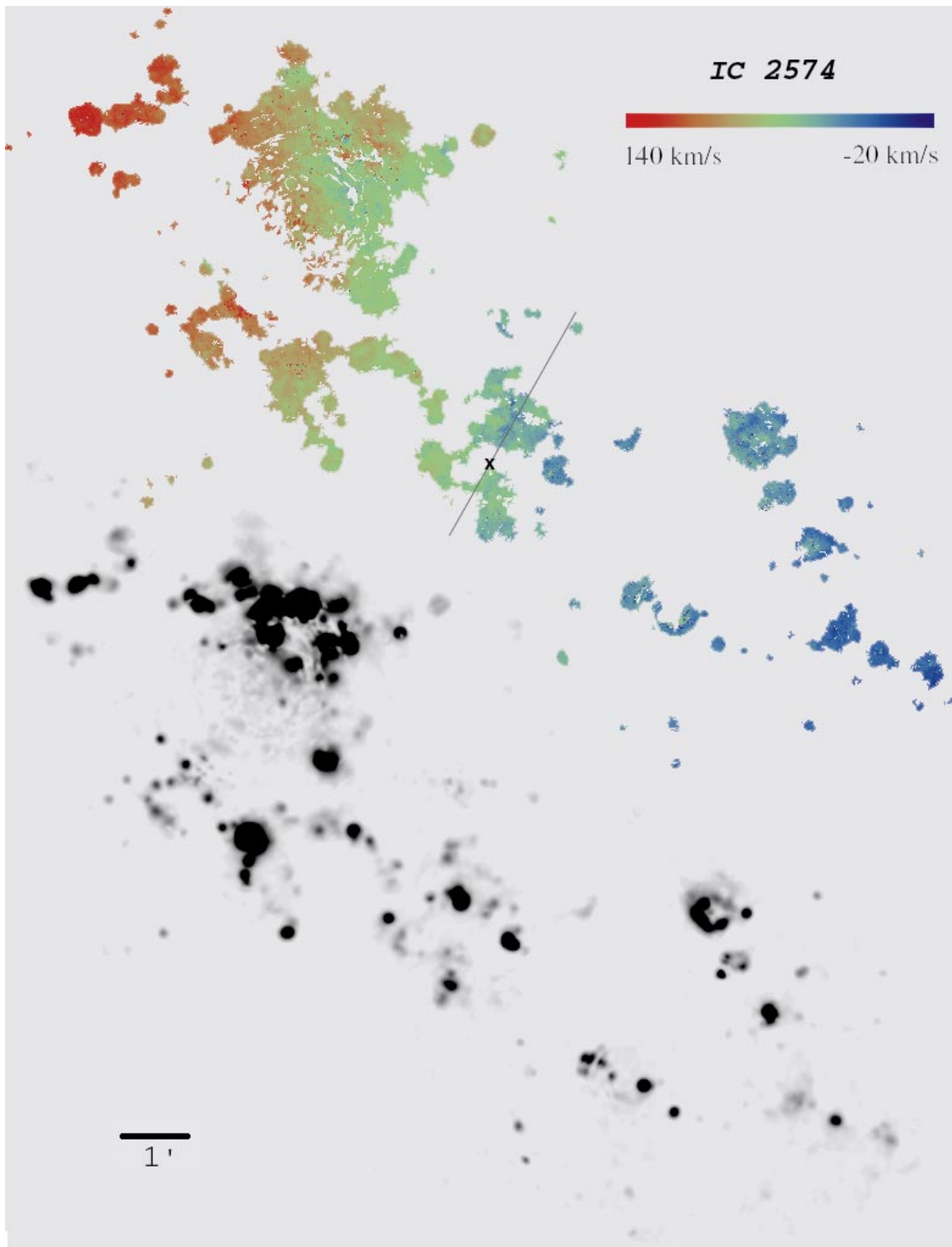


FIG. 3.—Velocity field and H $\alpha$  image of IC 2574. North is up and east is left. The X and the gray line indicate, respectively, the kinematic center and the axis of separation between the approaching and receding sides.

ations of radio telescopes (single dish and aperture synthesis). It confirms the great difficulty of reconciling a cuspy profile with  $\gamma \geq 1$  and the rotation curve of a late-type spiral like NGC 3109. Either constant-density core profiles or mildly cuspy profiles with  $\gamma \ll 1$  can fit the data adequately. It is very difficult to discriminate between a density distribution with a flat core from one with a mild cusp because  $r_0$  can often be stretched to a point where the two types of profile match. One really has to go to very small radii ( $\lesssim \gamma r_0$ ) to probe any incompatibility.

Cuspy profiles with  $\gamma \geq 1$  seem to appear generically in cold dark matter (CDM)  $N$ -body simulations, but many models have been suggested that deviate somewhat from the standard CDM assumptions and avoid the creation of a steep central density cusp. As noted by KKBP, Syer & White (1998) showed that  $\gamma$  is sensitive to the past merger rate and to the power spectrum of the initial density fluctuations on the scale of a galactic halo. Therefore a less active merger history or a steeper power spectrum should lead to  $\gamma < 1$  on galactic scales. Recently, however (Kravtsov et al.

TABLE 5  
OPTICAL ROTATION CURVE OF IC 2574 AT 9% BINNING FROM ADHOC

R (arcsec)	$N_{\text{app}}$	$V_{\text{app}}$ ( $\text{km s}^{-1}$ )	$\sigma_{\text{ring}}$ ( $\text{km s}^{-1}$ )	$N_{\text{rec}}$ ( $\text{km s}^{-1}$ )	$V_{\text{rec}}$ ( $\text{km s}^{-1}$ )	$\sigma_{\text{ring}}$ ( $\text{km s}^{-1}$ )	$V$ ( $\text{km s}^{-1}$ )
8 .....	...	...	...	2	22	8	$22 \pm 5$
12 .....	...	...	...	3	34	9	$34 \pm 5$
15 .....	22	8	20	...	...	...	$8 \pm 4$
24 .....	36	15	10	79	10	7	$11 \pm 1$
33 .....	26	12	12	81	3	27	$5 \pm 3$
43 .....	22	2	10	...	...	...	$2 \pm 2$
52 .....	62	10	15	144	3	22	$5 \pm 2$
61 .....	101	17	22	206	6	17	$10 \pm 2$
70 .....	139	27	24	228	9	16	$16 \pm 1$
80 .....	151	30	29	200	14	14	$21 \pm 2$
89 .....	113	42	37	202	16	16	$25 \pm 2$
99 .....	62	43	23	174	29	13	$33 \pm 2$
108 .....	75	33	23	157	30	16	$31 \pm 2$
118 .....	78	31	25	144	32	20	$32 \pm 2$
127 .....	72	33	27	137	31	19	$32 \pm 2$
137 .....	53	53	28	206	25	12	$30 \pm 2$
146 .....	40	66	26	423	26	9	$30 \pm 1$
155 .....	41	79	33	646	28	8	$31 \pm 1$
165 .....	45	54	40	739	31	13	$32 \pm 2$
174 .....	68	37	46	734	32	11	$33 \pm 2$
183 .....	81	25	18	712	34	10	$33 \pm 1$
193 .....	94	30	15	593	36	6	$35 \pm 1$
202 .....	102	31	22	510	36	8	$35 \pm 1$
212 .....	141	32	29	457	37	12	$36 \pm 1$
221 .....	193	34	24	410	40	13	$38 \pm 1$
230 .....	155	30	22	309	44	16	$40 \pm 1$
240 .....	147	42	34	418	48	12	$47 \pm 2$
249 .....	139	42	34	487	48	14	$46 \pm 1$
259 .....	185	43	28	497	46	15	$45 \pm 1$
268 .....	190	40	21	372	43	12	$42 \pm 1$
278 .....	138	44	23	234	40	21	$41 \pm 2$
287 .....	245	39	20	262	34	19	$36 \pm 1$
296 .....	287	44	13	258	34	28	$39 \pm 1$
306 .....	289	42	10	279	45	24	$44 \pm 1$
314 .....	279	38	11	218	42	23	$40 \pm 1$
325 .....	188	36	20	172	40	24	$38 \pm 2$
334 .....	347	37	20	195	45	31	$40 \pm 2$
343 .....	258	36	20	177	45	29	$40 \pm 2$
352 .....	159	40	13	183	47	27	$44 \pm 2$
362 .....	182	42	8	181	44	24	$43 \pm 1$
372 .....	327	44	15	175	46	23	$45 \pm 1$
381 .....	440	43	12	205	47	25	$45 \pm 1$
390 .....	255	40	18	217	53	28	$46 \pm 2$
400 .....	225	39	20	223	49	25	$44 \pm 2$
409 .....	162	41	29	291	52	26	$48 \pm 2$
418 .....	174	47	20	360	57	29	$54 \pm 1$
428 .....	162	50	42	424	60	32	$57 \pm 2$
437 .....	159	52	33	446	58	36	$57 \pm 2$
446 .....	171	46	31	367	55	27	$52 \pm 2$
456 .....	167	52	25	317	45	24	$48 \pm 2$
466 .....	173	55	23	343	48	28	$51 \pm 2$
475 .....	224	55	29	332	52	30	$53 \pm 2$
484 .....	240	59	45	339	54	28	$56 \pm 2$
494 .....	214	60	28	363	59	28	$59 \pm 2$
503 .....	171	64	36	434	60	22	$61 \pm 2$
512 .....	126	77	33	437	58	31	$62 \pm 2$
522 .....	96	70	15	504	59	37	$61 \pm 2$
531 .....	87	63	12	519	63	36	$63 \pm 2$
540 .....	85	73	32	511	62	37	$64 \pm 2$
550 .....	90	81	45	537	64	41	$66 \pm 2$
559 .....	65	71	30	505	65	39	$66 \pm 2$
568 .....	36	77	17	549	68	36	$68 \pm 2$
578 .....	17	85	25	553	64	35	$65 \pm 2$
587 .....	18	81	4	517	63	35	$64 \pm 2$

TABLE 5—Continued

R (arcsec)	$N_{\text{app}}$	$V_{\text{app}}$ ( $\text{km s}^{-1}$ )	$\sigma_{\text{ring}}$ ( $\text{km s}^{-1}$ )	$N_{\text{rec}}$ ( $\text{km s}^{-1}$ )	$V_{\text{rec}}$ ( $\text{km s}^{-1}$ )	$\sigma_{\text{ring}}$ ( $\text{km s}^{-1}$ )	$V$ ( $\text{km s}^{-1}$ )
595.....	3	79	4	433	55	42	$55 \pm 2$
606.....	...	...	...	465	60	38	$60 \pm 2$
616.....	...	...	...	496	67	36	$67 \pm 2$
625.....	...	...	...	521	76	37	$76 \pm 2$
634.....	...	...	...	531	79	35	$79 \pm 2$
645.....	8	60	78	518	82	36	$82 \pm 4$
653.....	19	101	75	513	82	41	$82 \pm 4$
663.....	...	...	...	478	71	43	$71 \pm 2$
672.....	...	...	...	476	70	36	$70 \pm 2$
682.....	...	...	...	462	69	42	$69 \pm 2$
691.....	...	...	...	465	78	38	$78 \pm 2$
700.....	...	...	...	465	88	38	$88 \pm 2$
710.....	...	...	...	460	87	39	$87 \pm 2$
719.....	...	...	...	421	83	31	$83 \pm 1$
728.....	...	...	...	348	85	29	$85 \pm 2$
738.....	...	...	...	342	94	20	$94 \pm 1$
747.....	...	...	...	323	94	20	$94 \pm 1$
757.....	...	...	...	282	95	24	$95 \pm 1$
766.....	...	...	...	280	93	25	$93 \pm 2$
776.....	...	...	...	255	92	34	$92 \pm 2$
785.....	...	...	...	268	97	33	$97 \pm 2$
794.....	...	...	...	277	97	40	$97 \pm 2$
803.....	...	...	...	215	99	46	$99 \pm 3$
813.....	...	...	...	163	101	42	$101 \pm 3$
823.....	...	...	...	115	110	32	$110 \pm 3$
869.....	...	...	...	61	120	14	$119 \pm 2$
877.....	...	...	...	24	103	12	$102 \pm 2$

NOTES.—Derived with  $V_{\text{sys}} = 53 \text{ km s}^{-1}$ ,  $i = 75^\circ$ , and P.A. =  $52^\circ$ . The two sides are computed independently, and the total is their mean averaged by the number of points. The velocity dispersion and the number of points appear for both sides, while the error is  $\sigma/\sqrt{N}$  of the two sides, added in quadrature.

2000), KKBP withdrew their  $N$ -body simulation results. Thus, their density profiles used here should not be considered a product of CDM simulations.

Self-interacting dark matter (Spergel & Steinhardt 2000) has also been suggested to suppress the formation of high-density dark matter cusps, but the implied inverse dependency of the core radius on the mass of the galaxy (Dalcanton & Hogan 2000) is not observed in our sample.

Alternatively, in order to explain the presence of a flat-density core in dwarf spiral galaxies for standard, scale-free CDM models, Navarro, Eke, & Frenk (1996a) suggested that a violent starburst could eject the gas and consequently flatten the inner dark matter distribution. Semianalytical calculations give this scenario the right order of magnitude for a low-mass galaxy, given a sufficient feedback efficiency (van den Bosch et al. 2000).

Another way to reconcile the too steep rotation curves without invoking a flat-density CDM core is to add a second dark component, composed of compact objects, to the nonbaryonic cold dark matter (Burkert & Silk 1997). Of

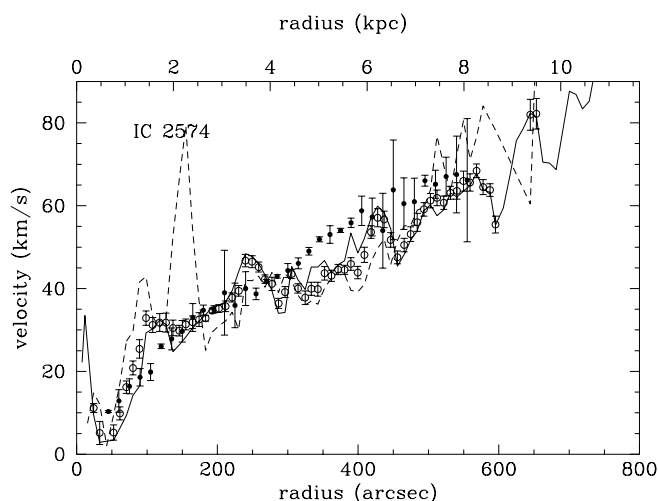


FIG. 4.— $\text{H}\alpha$  rotation curve of IC 2574 (open circles) compared with the HI rotation curve (filled circles) from Martimbeau, Carignan, & Roy (1994), showing the approaching (dashed line) and receding (continuous line) sides of the  $\text{H}\alpha$  curve.

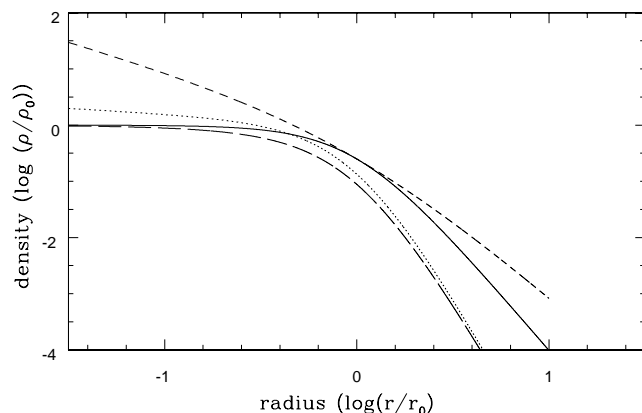


FIG. 5.—Density profiles of the four models: pseudoisothermal sphere (solid line), KKBP (dotted line), Burkert (long-dashed line), and NFW (short-dashed line).

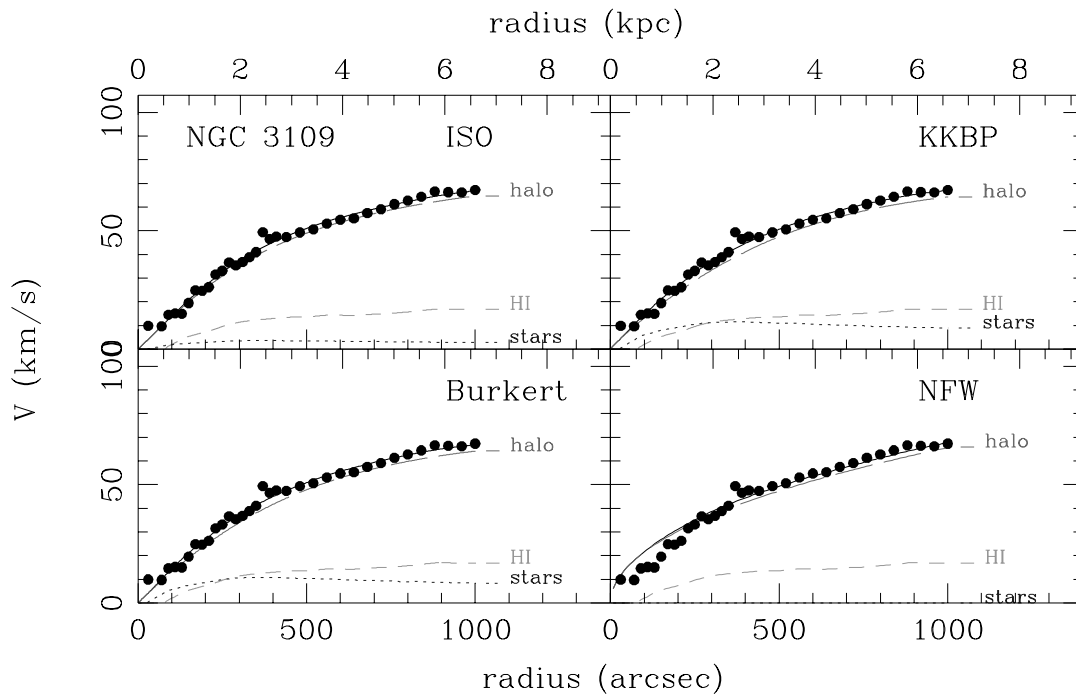


FIG. 6.—Best-fit mass models for NGC 3109, using the H $\alpha$  rotation curve up to 2.7 kpc and the H I rotation curve for the rest, showing dark halo density profiles for the pseudoisothermal sphere (*top left*), KKBP (*top right*), Burkert (*bottom left*), and NFW (*bottom right*). [See the electronic edition of the *Journal* for a color version of this figure.]

course, this adds some degrees of freedom when fitting rotation curves and a better fit is in this case somewhat meaningless, making this hypothesis hard to test. The present knowledge of the importance and distribution of massive compact halo objects (MACHOs) in our own Galaxy allows them to account for around 20% (up to 50% at a 95% confidence level) of the galactic dark matter (Alcock et al.

2000). In any case, this is barely enough to solve the cusp problem. Indeed, the MACHOs would need a very finely tuned distribution.

NGC 5585 is also well fitted by all the profiles but those in NFW (Fig. 8). The slight difference between the  $(M/L_B)_*$  found here (0.85) and the one found in Paper I (0.80) is due to the use of equation (1) instead of the integration of the

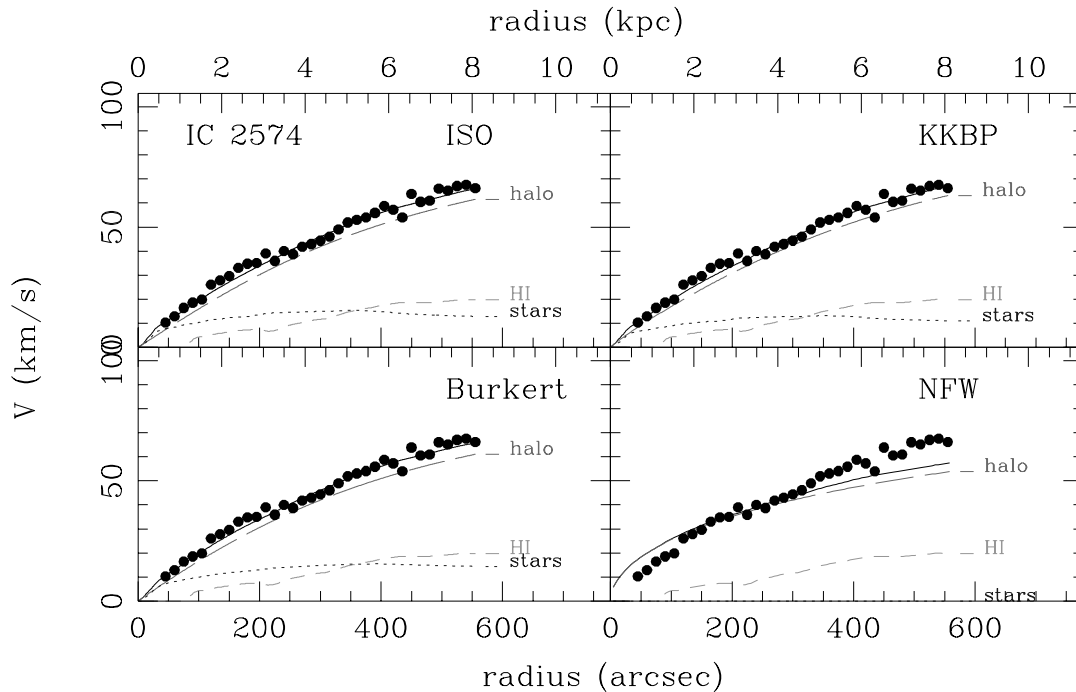


FIG. 7.—Mass models of IC 2574, using the H I rotation curve only. [See the electronic edition of the *Journal* for a color version of this figure.]

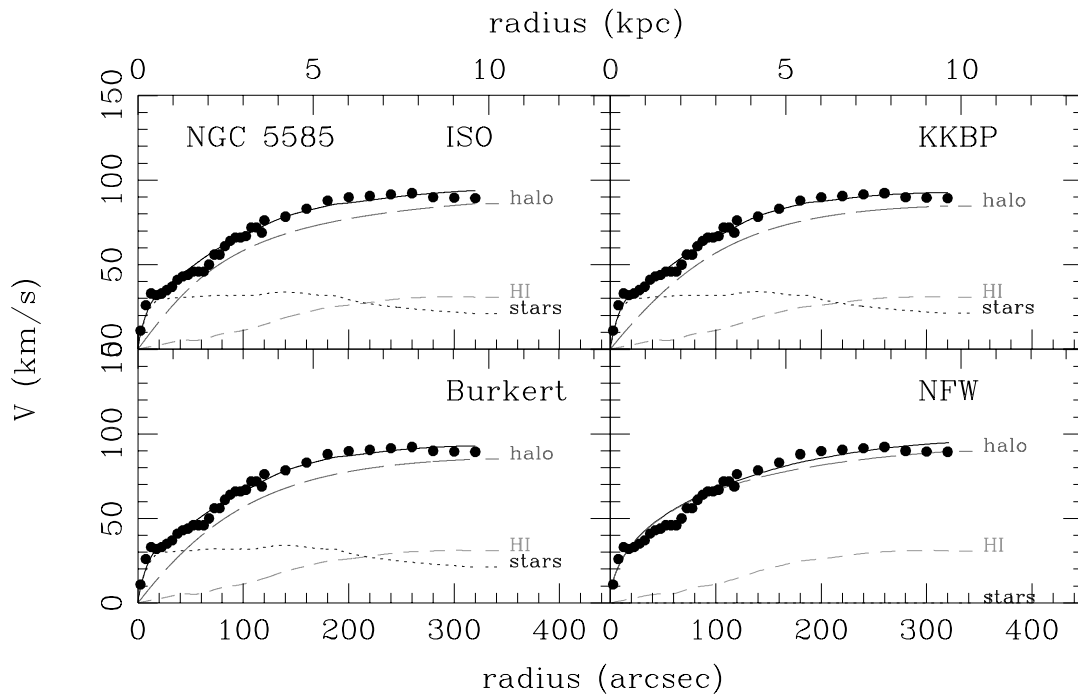


FIG. 8.—Mass models of NGC 5585, using the  $H\alpha$  rotation curve up to 3.5 kpc and H I for the rest. [See the electronic edition of the Journal for a color version of this figure.]

appropriate Lane-Emden equation for the isothermal sphere.

In the case of NGC 3198 (Fig. 9), all the profiles are compatible. The  $H\alpha$  curve has been used up to  $65''$  to rectify the overcorrection of the beam smearing in Begeman (1987). The only remark to be made is that all the profiles are too smooth to account for the small variations in the outer rotation curve, even though they are present in both the H I

and the B profile. The detailed gravitational interplay between luminous and dark matter should be taken into account. The detailed results of the mass models can be found in Table 6.

### 3.2. Modified Newtonian Dynamics

Milgrom (1983) proposed that a modification of Newtonian gravitation in the low-acceleration limit could mimic a

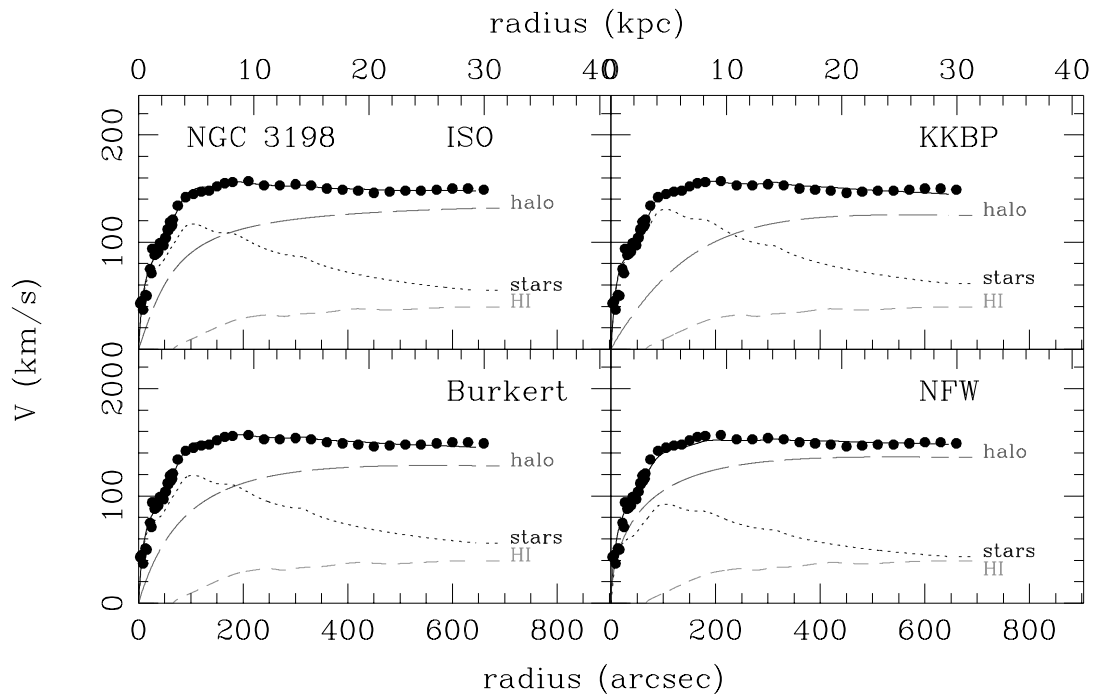


FIG. 9.—Mass models of NGC 3198, using the  $H\alpha$  rotation curve up to 2.9 kpc and H I for the rest. [See the electronic edition of the Journal for a color version of this figure.]

TABLE 6  
PARAMETERS OF THE MASS MODELS

Model and Galaxy	Type	( $M/L_B$ ) <sub>*</sub>	$r_0$ (kpc)	$\rho_0$ ( $10^{-3}M_\odot/\text{pc}^{-3}$ )	$c$	$\chi^2$
ISO:						
IC 2574.....	SABm	0.34	5.4	7.0	10	2.7
NGC 3109.....	SBm	0.04	2.4	2.5	6.6	2.8
NGC 5585.....	SABd	0.85	2.2	4.3	8.2	4.4
NGC 3198.....	SBC	4.8	2.5	5.7	9.2	7.1
Burkert:						
IC 2574.....	...	0.6	8.0	8.4	11	2.5
NGC 3109.....	...	0.35	4.1	2.5	6.6	2.9
NGC 5585.....	...	0.086	4.0	4.0	8.0	8.2
NGC 3198.....	...	5.0	5.8	7.4	10	7.7
KKBP:						
IC 2574.....	...	0.25	9.2	5.0	8.8	2.4
NGC 3109.....	...	0.40	4.5	1.5	5.2	2.9
NGC 5585.....	...	0.86	3.9	5.6	9.2	7.4
NGC 3198.....	...	6.0	9.2	1.2	4.7	9.1
NFW:						
IC 2574.....	...	0.0	35	0.05	1.0	44
NGC 3109.....	...	0.0	109	0.024	0.61	10
NGC 5585.....	...	0.0	10.1	0.77	3.9	7.9
NGC 3198.....	...	3.0	11.2	1.3	4.9	44

NOTES.—Model parameters  $r_0$  and  $\rho_0$  are, respectively, the characteristic radius and characteristic density. The concentration  $c$  is calculated following Navarro et al. (1996b) and is exact only in the NFW case. Because of the model dependence,  $c$  is only approximate for the other cases.

large amount of dark matter in spiral galaxies. The modified Newtonian dynamics (MOND) is a truly falsifiable theory: it contains only one parameter,  $a_0$ , that is supposed to be a universal constraint. A lot of work has been done using rotation curves for which the quality of the data gives the best opportunity to test the theory (e.g., Begeman, Broeils, & Sanders 1991; Sanders 1996; Sanders & Verheijen 1998; McGaugh & De Blok 1998).

As a reminder, here is the MOND quantitative prescription. For purely circular motion, one can equate the centripetal and gravitational accelerations. In the Newtonian regime, we simply get

$$\frac{V^2}{R} = \frac{GM_T}{R^2} = g_N \quad (2)$$

MOND states that the true force is given by

$$\mu(g/a_0)g = g_N \quad (3)$$

where  $\mu(g/a_0)$  is an interpolation function that has the right asymptotic behavior:  $\mu(g/a_0 \gg 1) \rightarrow 1$  and  $\mu(g/a_0 \ll 1) \rightarrow g/a_0$ .

The exact form of  $\mu(g/a_0)$  has no impact on the mass models of very late-type spiral galaxies such as NGC 3109 and IC 2574 where the gravitational acceleration is well below  $a_0$  at all radii, but

$$\mu(x) = \frac{x}{\sqrt{1+x^2}} \quad (4)$$

is generally assumed to be the interpolation function.

In the limit of low acceleration the gravitational acceleration is thus given by  $g = \sqrt{a_0 g_N}$  and

$$\frac{V^2}{R} = \sqrt{\frac{GM_T}{R^2} a_0} \quad (5)$$

or

$$V^4 = GM_T a_0 \quad (6)$$

which naturally explains the asymptotic flatness of rotation curves and the Tully-Fisher relation.

A best-fit method similar to the one used for dark halos has been applied. The stellar luminosity profile and the H I density profile are this time transformed into a mass distribution following equations (3) and (4). The free parameter of the fit is as always the ratio ( $M/L$ )<sub>\*</sub>;  $a_0$  is considered a universal constant, but, since no fundamental theory exists yet to give its true value, two different values are used in the fits. The first value was found by Begeman et al. (1991) and best fits their highly selective and high-quality sample of luminous spiral galaxies ( $1.2 \times 10^{-13} \text{ km s}^{-1}$ ). The second value is the one that best fits each present galaxy individually (Table 7). Figure 10 shows the best fit for each galaxy, and Table 7 indicates the parameters when using the best-fitted  $a_0$ .

IC 2574, NGC 3109, and NGC 3198 are fairly well fitted by the MOND law if the “universal constant”  $a_0$  is allowed to vary by more than a factor 2. The quality of the fit is especially good in the case of IC 2574, where most of the features of the rotation curve are reproduced in the fit. On the other side, the MOND prescription has more difficulties to account for the mass distribution of NGC 5585 whatever

TABLE 7  
MOND PARAMETERS WITH THE BEST-FITTED  $a_0$

Galaxy	Distance (Mpc)	$a_0$ ( $\times 10^{-13} \text{ km s}^{-2}$ )	( $M/L_B$ ) <sub>*</sub>	$\chi^2$ ( $M_\odot/L_\odot$ )
IC 2574	3.0	2.0	0.02	1.5
NGC 3109	1.36	1.7	0.0	2.0
NGC 5585	6.2	2.5	0.34	5.9
NGC 3198	9.36	0.9	6.7	1.1

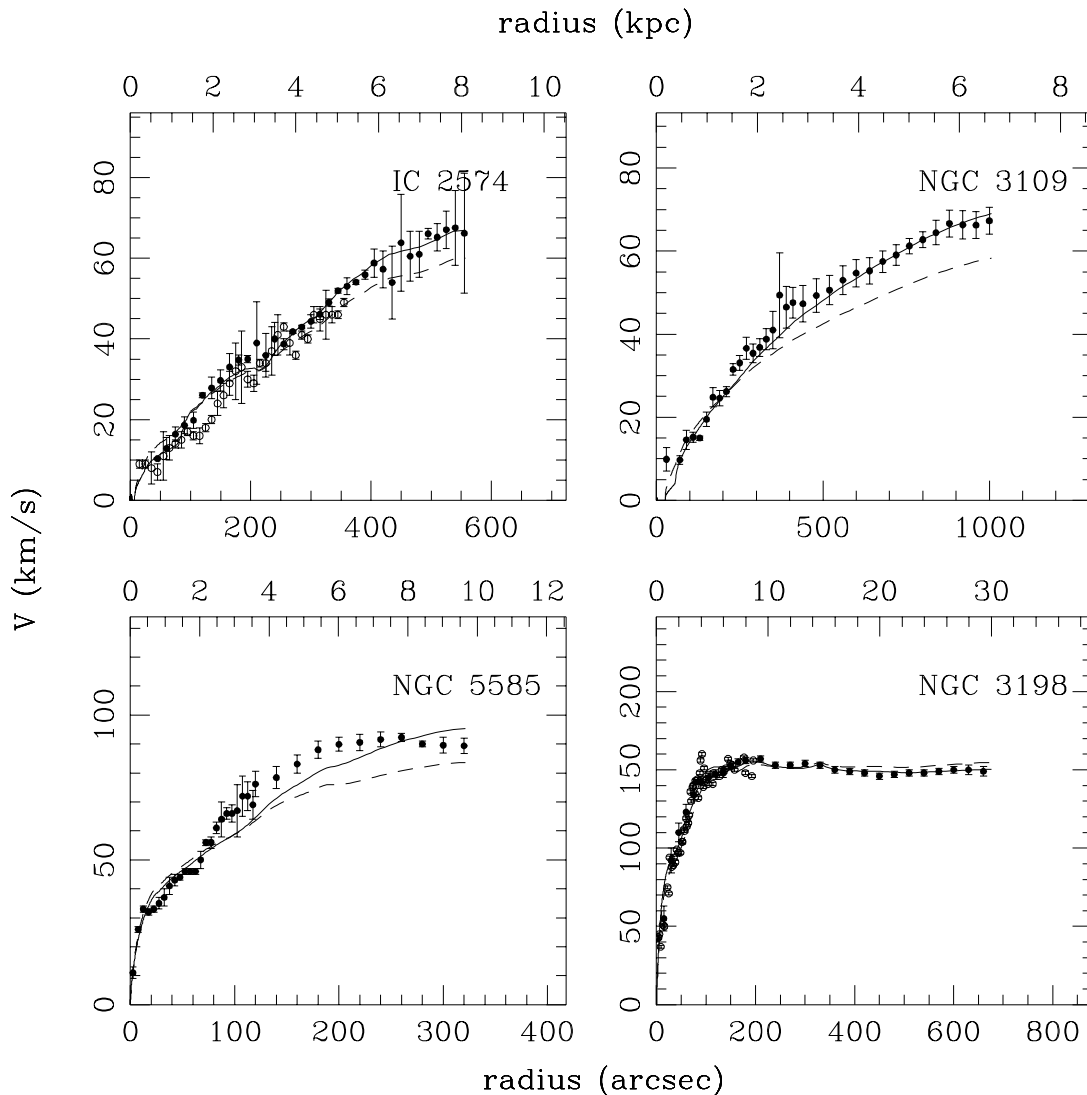


FIG. 10.—Best-fit mass models using MOND and two different values of  $a_0$ :  $a_0 = 1.2 \times 10^{-13} \text{ km s}^{-12}$  from Begeman, Broeils, & Sanders 1991; (*dotted line*) and the best-fit value (see Table 7; *continuous line*). Filled circles represent the data used in the fits (H I + H $\alpha$  for NGC 3109 and 5585 and H I only for IC 2574 and NGC 3198). Open circles indicate H $\alpha$  velocities not used in the fits.

the value of  $a_0$ . Being for a large part in the Newtonian regime, the case of NGC 5585 is somewhat less significant as it probes the interpolation function more than the MOND theory itself. In contrast, NGC 3109 fully belongs to the MOND regime. In this case, using new Australia Telescope Compact Array H I data improves significantly the MOND fit compared with the one obtained with the old VLA data (the  $\chi^2$  goes from 5 to 2), which were missing  $\frac{1}{3}$  of the flux.

#### 4. SUMMARY AND DISCUSSION

With the four galaxies studied so far, it is clear that while there is a good agreement between Fabry-Perot and H I data for the shallow rotation curves of the late-type galaxies NGC 3109 and IC 2574, beam smearing plays an important role for the steeper rotation curves. Beam smearing thus seems to depend on at least two factors: the inner slope of the rotation curve and the sampling of the curve, often expressed as the ratio of the Holmberg radius to the beam width (Bosma 1978). Bosma suggested a ratio greater than 6 to have a reliable H I curve. This ratio is about 7 for NGC

5585 and 30 for NGC 3109, and the latter is still slightly affected by beam smearing.

Using multiwavelength rotation curves to determine the density profiles of dark matter halos, it appears clearly that cuspy profiles with inner logarithmic slope  $\gamma \geq 1$  do not match the observations. The best fits are achieved using either a slightly cuspy profile with a very shallow inner slope or a profile with a flat-density core. If current simulations correctly describe CDM evolution, an additional process is needed to destroy or forbid the formation of a central cusp. However, none of the actually proposed scenarios stand out as the most plausible, either because they are not easily testable or their predictions do not appear clearly in the data.

The modified Newtonian dynamics prescription can fit the rotation curves of IC 2574, NGC 3109, and NGC 3198 obtained from the new high-resolution data if  $a_0$  is free to vary by a factor of 2. In this case, most of the features of the rotation curve are even reproduced with the right amplitude. Of course, since there is almost no stellar disk, at least in the part fully in the MOND regime, scaling the H I would

produce a similar result. Can  $H_2$  be involved here? (Pfenniger, Combes, & Martinet 1994). On the other hand, possibly the variations of the stellar and gaseous components also just follow a nonsmooth dark matter distribution.

There is always a danger to let what should be a universal constant like  $a_0$  vary to fit the data. However, since no underlying theory exists yet, it is interesting to note that for these late-type spiral galaxies,  $a_0$  seems systematically higher than for the earlier types.

## 5. CONCLUSION

The present work leads to the following conclusions:

1. Observations of the kinematics of the ionized hydrogen in NGC 3109 and IC 2574 are in good agreement with the previous kinematical studies of atomic hydrogen. This implies that beam smearing was limited in the H I data, although NGC 3109 was slightly affected.

2. Overall, beam smearing can be important even for “good sampling,” depending on the inner slope of the rotation curve.

3. The CDM models with an inner density slope  $\gamma \geq 1$  are not compatible with the data on NGC 3109 and IC 2574. Flat-density core models like the pseudoisothermal

sphere or a model with a shallow inner density slope are compatible with the four galaxies in our sample.

4. With the exception of NGC 5585, the MOND prescription can fit the rotation curves of the three other galaxies in our sample if the universal constant  $a_0$  is allowed to vary by more than a factor of 2. The  $a_0$  values found for the late-type galaxies are systematically higher than that found previously for more massive spiral galaxies.

The present examples give a good idea of the impact of higher resolution rotation curves. There are however large unexplored regions in terms of galaxy mass, surface brightness, and morphological types. It is thus imperative to extend this sample to earlier type galaxies covering a large range in surface brightness. This would give, among other things, the opportunity to study precisely at what point the rotation curves stop agreeing with  $N$ -body simulations.

We would like to thank the staff of the CFHT for their support during the data acquisition and Daniel Durand from Hertzberg Institute for Astrophysics, who helped with data acquisition. We also warmly thank Jacques Boulesteix for fruitful discussion on Fabry-Perot reduction and Piotr Popowski for valuable comments. C. C. acknowledges grants from NSERC (Canada) and FCAR (Québec).

## REFERENCES

- Alcock, C., et al. 2000, *ApJ*, 542, 281  
 Amram, P., Marcelin, M., Boulesteix, J., & Le Coarer, E. 1992, *A&A*, 266, 106  
 Begeman, K. 1987, Ph.D. thesis, Groningen Univ.  
 Begeman, K. G., Broeils, A. H., & Sanders, R. H. 1991, *MNRAS*, 249, 523  
 Blais-Ouellette, S., Carignan, C., Amram, P., & Côté, S. 1999, *AJ*, 118, 2123 (Paper I)  
 Bosma, A. 1978, Ph.D. thesis, Groningen Univ.  
 Broeils, A. 1992, Ph.D. thesis, Groningen Univ.  
 Burkert, A. 1995, *ApJ*, 447, L25  
 Burkert, A., & Silk, J. 1997, *ApJ*, 488, L55  
 Carignan, C., & Freeman, K. C. 1985, *ApJ*, 294, 494  
 Casertano, S. 1983, *MNRAS*, 203, 735  
 Côté, S., Carignan, C., & Sancisi, R. 1991, *AJ*, 102, 904  
 Dalcanton, J. J., & Hogan, C. J. 2000, preprint (astro-ph/0004381)  
 de Vaucouleurs, G., de Vaucouleurs, A., Corwin, H. G., Buta, R. J., Paturel, G., & Fouque, P. 1991, *Third Reference Catalogue of Bright Galaxies*, Vol. 1–3, 12 (Berlin: Springer)  
 Fukushige, T., & Makino, J. 1997, *ApJ*, 477, L9  
 Jobin, M., & Carignan, C. 1990, *AJ*, 100, 648  
 Kent, S. M. 1987, *AJ*, 93, 816  
 Kravtsov, A. V., Klypin, A. A., Bullock, J. S., & Primack, J. R. 1998, *ApJ*, 502, 48 (KKBP)  
 Kravtsov, A. V., Klypin, A. A., Bullock, J. S., & Primack, J. R. 2000, preprint (astro-ph/0006343)  
 Martimbeau, N., Carignan, C., & Roy, J.-R. 1994, *AJ*, 107, 543  
 McGaugh, S. S., & De Blok, W. J. G. 1998, *ApJ*, 499, 41  
 Milgrom, M. 1983, *ApJ*, 270, 365  
 Moore, B., Governato, F., Quinn, T., Stadel, J., & Lake, G. 1998, *ApJ*, 499, L5  
 Musella, I., Pionto, G., & Capaccioli, M. 1997, *AJ*, 114, 976  
 Navarro, J. F. 1997, in *ASP Conf. Ser. 117, Dark and Visible Matter in Galaxies and Cosmological Implications*, ed. M. Persic & P. Salucci (San Francisco: ASP), 404  
 Navarro, J. F., Eke, V. R., & Frenk, C. S. 1996a, *MNRAS*, 283, L72  
 Navarro, J. F., Frenk, C. S., & White, S. D. M. 1996b, *ApJ*, 462, 563  
 ———. 1997, *ApJ*, 490, 493  
 Pfenniger, D., Combes, F., & Martinet, L. 1994, *A&A*, 285, 79  
 Sanders, R. H. 1996, *ApJ*, 473, 117  
 Sanders, R. H., & Verheijen, M. A. W. 1998, *ApJ*, 503, 97  
 Spergel, D., & Steinhardt, P. 2000, *Phys. Rev. Lett.*, 84, 3760  
 Syer, D., & White, S. D. M. 1998, *MNRAS*, 293, 337  
 van den Bosch, F. C., Robertson, B. E., Dalcanton, J. J., & de Blok, W. J. G. 2000, *AJ*, 119, 1579  
 Zhao, H. 1996, *MNRAS*, 278, 488